The Output Characteristics of Transcranial Magnetic Stimulation with Voltage Variable Capacitor-Charging System

Whi-Young Kim, *Member, KIMICS*

Abstract— **In this study, a Magnetic stimulation Pulse Train control technique is introduced and applied to Flyback converter operating in discontinuous conduction mode. In contrast to the conventional pulse width modulation control scheme, the principal idea of a Magnetic stimulation Pulse Train is to achieve output voltage regulation using high and low power pulses. The proposed technique is applicable to any converter operating in discontinuous conduction. However, this work mainly focuses on Flyback topology. In this paper, the main mathematical concept of the new control algorithm is introduced and simulations as well as experimental results are presented.**

Index Terms—non-invasive, neuro-imaging, brain, electroence phalography (EEG), magnetoence phalography (MEG), positron emission tomography (PET), near-infrared spectroscopy (NIRS), fMRI, transcranial magnetic brain stimulation (TMS)

I. INTRODUCTION

The use of non-invasive neuro-imaging has been increased explosively in recent years. Details of the functioning of the human brain are revealed by measuring electromagnetic fields outside the head or metabolic and hemodynamic changes using electroence phalography (EEG), magnetoence phalography (MEG), positron emission tomography (PET), near-infrared spectroscopy (NIRS) or functional magnetic resonance imaging (fMRI). This paper deals with transcranial magnetic brain stimulation (TMS), which is a direct way of manipulating and interfering with the function of the cortex, thus complementing conventional neuro imaging. For this power level the most suitable isolated topology is the flyback converter.

These converters can provide either single or multiple outputs. Flyback converters are more suitable than forward converters for relatively low power levels because Block diagram of magnetic stimulation as shown in Fig 1. Their relative simplicity results from the elimination of the output inductor and freewheel diode that would be present in the secondary stage of a forward converter. The energy acquired by the transformer during the on-time of the primary IGBT is delivered to the output in the non-conducting period of the primary switch..

The secondary winding is connected with reverse polarity, so there can be no current flow to the output, due to the blocking diode. Since the number of semiconductor and magnetic components of Flyback converter is less than the other SMPS and, furthermore, it provides input/output isolation; therefore, this topology perfectly suits off-line low-cost power supply applications. Critical conduction mode enjoys benefits such as zero current turn-on of the switch and zero current turn-off of the freewheeling diode.

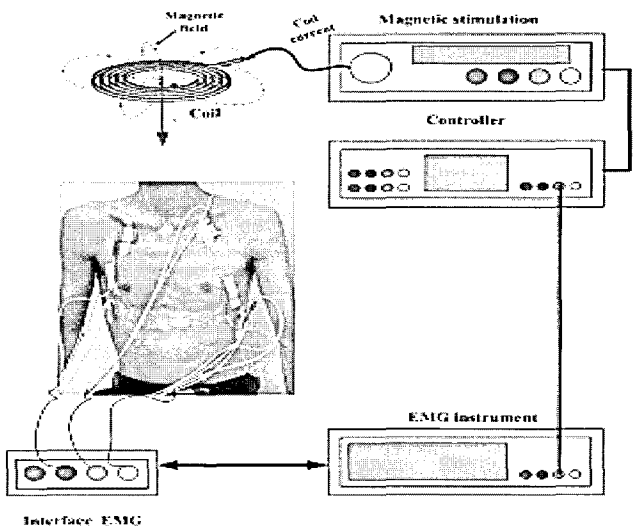

Fig. 1 Block diagram of magnetic stimulation

These soft switching transitions reduce the switching losses as well as the electromagnetic interference noise. Critical conduction mode has less current stress compared to DC. When the primary IGBT ceases to conduct, the induced voltage is reversed by the collapse of the magnetic field, and the output capacitor is charged through the diode. Since the circuit only requires one magnetic component the transformer flyback converters are simpler and cheaper than forward converters to design and build. However, despite the advantageous benefits of critical conduction mode, its major drawback is the variations of the switching frequency of the converter as the output load changes. This paper introduces a

Manuscript received March 8, 2010; revised March 17, 2010; accepted April 5, 2010.

Whi-Young Kim is with the Department of Biomedical Engineering, Dongju College Univesity, Busan, 604-715, Korea (Email: ndyag@dongju.ac.kr)

Transcranial Magnetic Stimulation Pulse Train control technique, which regulates the output voltage based on presence and absence of power and sense pulses and makes the Flyback converter operate in partial DC and partial critical conduction mode.

Not only does this control scheme offer a faster dynamic response compared with pulse width modulation method, but also improves the efficiency by lowering the switch turn-on loss at the end of each power pulse based on choosing the right turn-on time instant. The required information for this action is provided from the measured signals of the converter during the sense pulses. From a Transcranial Magnetic Stimulation Pulse Train is simple, cost effective, and robust against the variations of the parameters of the converter. A method that shows some similarity to a Transcranial Magnetic Stimulation Pulse Train technique was recently introduced with inferior characteristics. To achieve fixed frequency operation, proposes skip cycle modulation, which is basically an on/off control mode to regulate the output voltage.

II. CIRCUIT DESIGN

A Transcranial Magnetic Stimulation Pulse Train control algorithm regulates the output voltage based on the presence and absence of power pulses, rather than employing PWM.

Fig 2 depicts the block diagram of a transcranial magnetic stimulation pulse train regulation scheme. If the output voltage is higher than the desired level, low-power sense pulses are generated sequentially until the desired voltage level is reached. On the other hand, if the output voltage is lower than the desired level, instead of sense pulses, high-power power *pulses* are generated.

The time duration of the power and sense pulses are the same; but, due to the longer on time of the switch during a power pulse, compared to a sense pulse, more power will be delivered to the load.

The ratio between the on-time duration of the switch in a power pulse and the on-time duration of the switch in a sense pulse is chosen by making a compromise between the output voltage ripple and the power regulation range from full power to low power. Operating in constant peak current mode control, in a power pulse, the switch remains on and the primary current is allowed to increase until it reaches a designated constant peak level. At this point, the switch turns off and the next cycle starts when the secondary current reaches zero. The controller measures the time duration of the power pulses and makes the subsequent sense pulses to have the same time duration; hence the switching frequency of the converter is fairly constant when the load changes. A Transcranial Magnetic Stimulation Pulse Train enjoys on-line waveform analysis and hence, fast dynamic response.

III. HARDARE IMPLEMENTATION

The flyback converter in this circuit is designed to operate in discontinuous operation. To ensure this, the primary inductance Lp needs to be limited to a maximum value. Therefore, the maximum primary inductance for discontinuous conduction at maximum load needs to be determined. The input power is defined as

$$P_{IN}=\frac{P_{OUT}}{\eta} \quad \text{----------(1)}$$

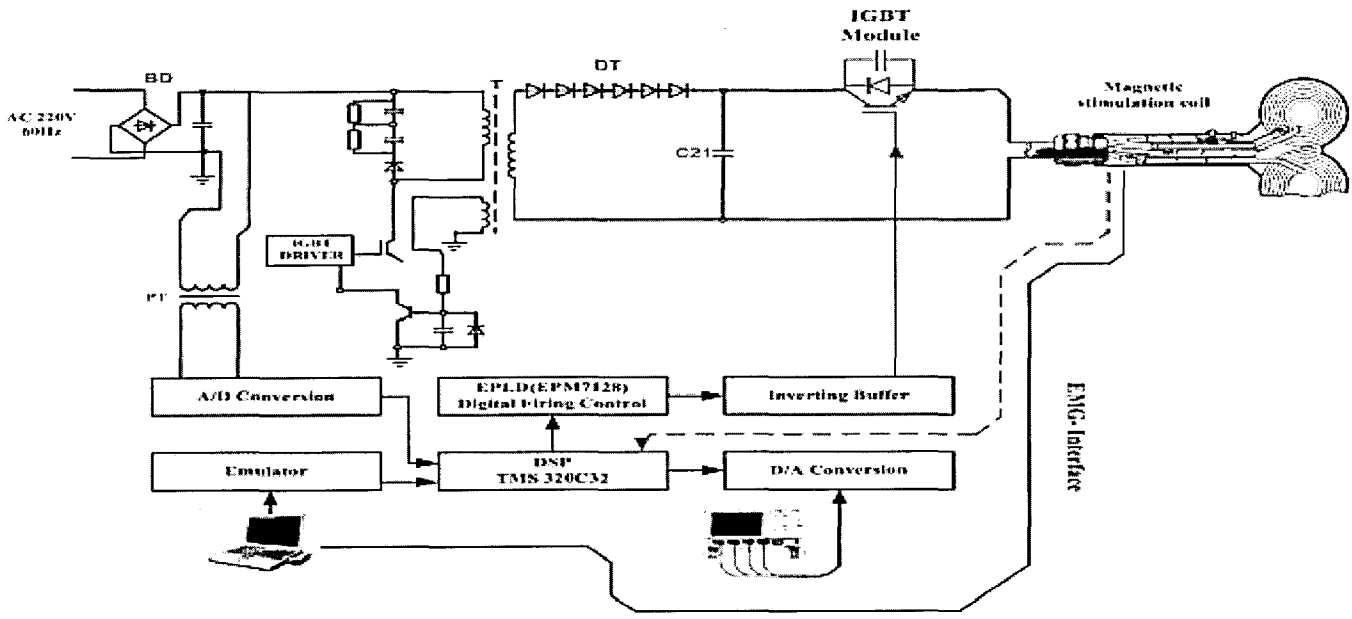

Fig. 2 The concept of a proposed flyback converter

where η is the efficiency of the inductor. The input power can also be defined as the product of the stored energy E in the magnetic field and the switching frequency fs

$$P_{IN} = Ef_s = \frac{L_p I^2 f_s}{2} \quad \text{----------(2)}$$

This allows the required primary inductance to be determined, but it is also necessary to know the peak current *Ipk* to be able to calculate this. The peak current is defined by 1.

$$L_{p(max)} = \frac{V^{2}_{in(min)} \delta^{2}_{max} T_s}{2P_{in(max)}} \quad \text{----------(3)}$$

where Vin(min) is the minimum supply voltage and ton(max) is the maximum on-time of the switch. Therefore, to limit the primary inductance to ensure discontinuous operation, the maximum inductance is determined, where δmax is the maximum duty cycle and Ts is the PWM switching period. By combining equations (2) and (4) it is possible to determine the maximum primary inductance

$$I_{pk} = \frac{V_{in(min)} t_{ON(max)}}{L_p}$$

$$L_{p(max)} \le \frac{V_{in(min)} t_{ON(max)}}{I_{pk}} = \frac{V_{in(max)}}{I_{pk}} \delta_{max} T_s \quad \text{---------(4)}$$

Considering a general switching period, as shown in Fig. 5, and based on the energy conservation rule, one can write

$$\Delta E_{in} = \Delta E_{L_m} + \Delta E_C + \Delta E_{Load} \quad \text{----------(5)}$$

where is the amount of energy that has been drawn from the input power source during the considered switching period. is the difference of the energy stored in the magnetizing inductance of the transformer and is equal to zero because de-energizes at the end of each switching period. is the change of the energy stored in the output capacitor during the same switching period and can be described as

$$\Delta E_C = E_{C,(n+1)T} - E_{C,nT} \quad \text{----------(6)}$$

And finally, is the amount of energy delivered to load during the same period. Output capacitor provides the load current; hence, we can write

$$\Delta E_{Load} = \frac{1}{R} \cdot \int_{nT}^{(n+1)T} V^2_o \cdot dt \quad \text{----------(7)}$$

In (7), using the trapezoidal rule instead of integration, we can approximate as with a flyback converter

$$\Delta E_{Load} \simeq \frac{T}{2R} (V^{2}_{o(n+1)T} + V^{2}_{onT} \quad \text{----------(8)}$$

Moreover, the energy stored in a capacitor at each instant is equal to the squared value of the voltage that appears across the capacitor divided by twice the value of the capacitor; hence, can be rewritten as

$$\Delta E_{Load} \simeq \frac{T}{RC} (E_{C,(n+1)T} + E_{CnT}) \quad \text{----------(9)}$$

Substituting (7) and (9) into (1) and solving for the energy stored in the output capacitor at the end of the desired switching period, one obtains

$$E_{C(n+1)T} = M \cdot E_{CnT} + \frac{1}{1+\frac{T}{RC}} \Delta E_{in} \quad \text{----------(10)}$$

$$M = \frac{1-\frac{T}{RC}}{1+\frac{T}{RC}} < 1 \quad \text{----------(11)}$$

Equation (11) shows the recursive relation of the energy stored in the output capacitor. Power

$$P = \frac{f_{train} (\Delta Wc)}{\eta} \quad \text{----------(12)}$$

f_{train} ΔWc η Where is the pulse train frequency, is the energy dissipated per pulse, and is the capacitor charger efficiency. The energy per pulse can be measured by subtracting the energy on all n capacitors in the power circuit before and after the pulse

$$\Delta Wc = \frac{1}{2} \sum_{i=1}^{n} CiV^2_{Ci}(t=0) - \frac{1}{2} \sum_{i=1}^{n} CiV^2_{Ci}(t \ge tp) \quad \text{----------(13)}$$

In expression (13), it is assumed that the capacitor charger is turned off or contributes a negligible amount of charge during the pulse. The stimulating coil temperature is proportional to square of the coil current integrated over the pulse duration, which is some times called the load integral

$$K_{coil} = \propto \int_0^{\ge tp} I_L^2 dt = \int_0^{p} I_L^2 dt + \int_p^{\ge tp} I_L^2 dt \quad \text{----------(14)}$$

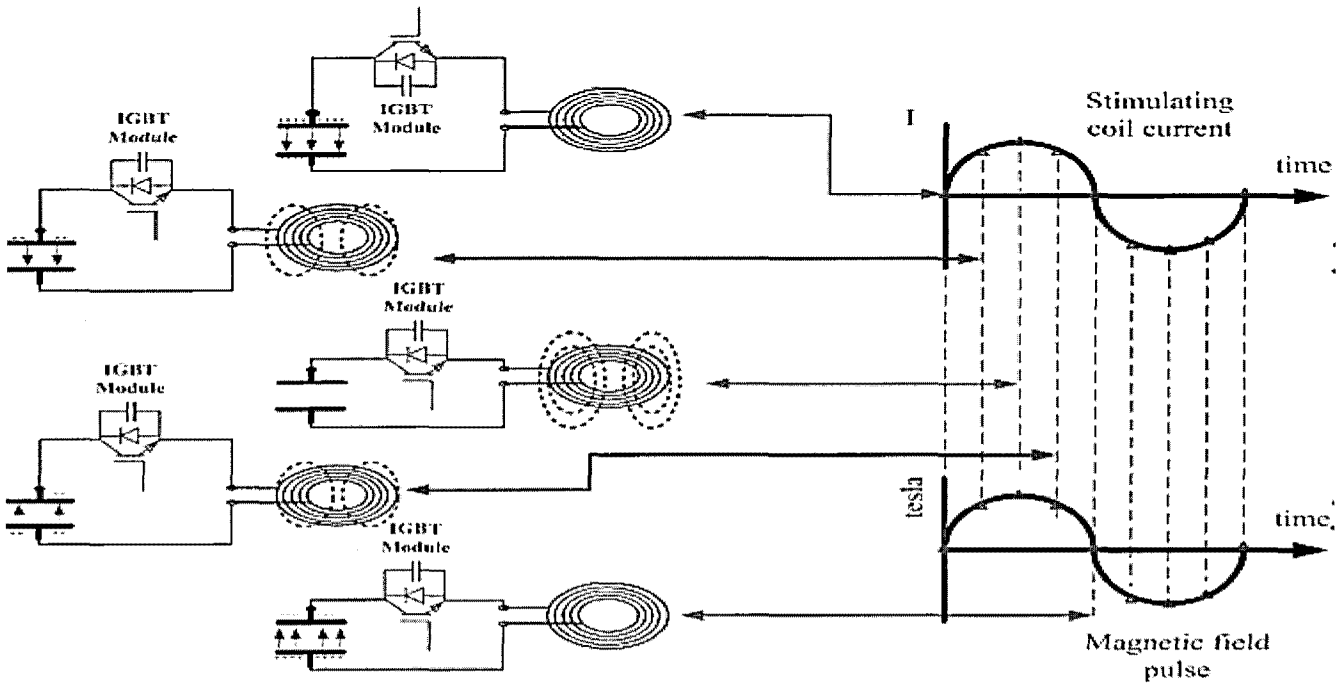

Fig. 3 Diagram of stimulating coil current

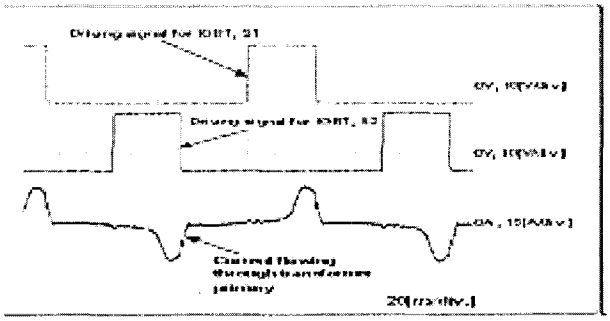

Fig. 4 Experimental waveforms for the collector- to-emitter voltage, current of S1 with their current and bypass current flowing through diode

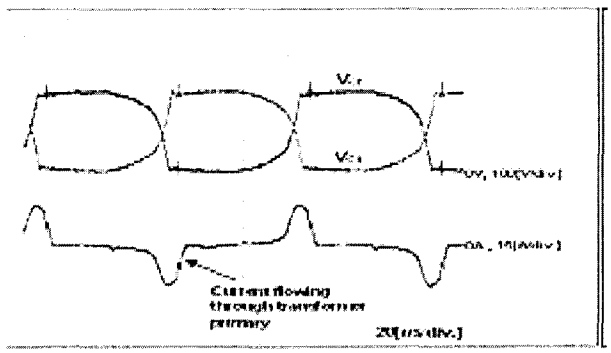

Fig. 5 Current waveform flowing through the transformer primary and voltage of the capacitor V_{C1} and V_{C2}

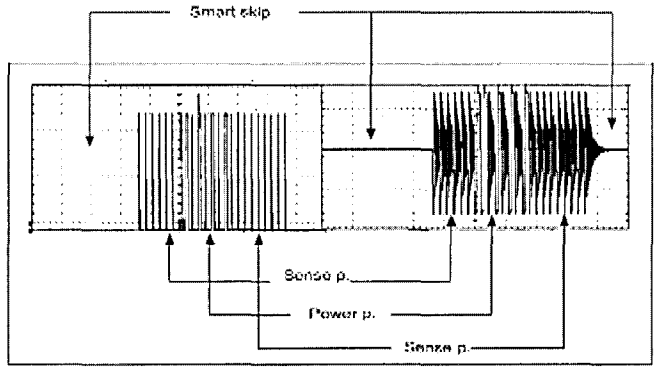

Fig. 6 Experimental waveforms for smart skip and pulse mode

Fig 3 indicated diagram of stimulating coil current, Fig 4 indicated experimental waveforms for the collector- to-emitter voltage, current, Fig 5 indicated current waveform flowing through the transformer primary and voltage, Fig 6 indicated experimental waveforms for smart skip and pulse mode. To compare the efficiency and coil heating of the near-rectangular Magnetic Stimulation electric field pulses to those of conventional stimulators, the Magnetic Stimulation device was reconfigure to produce damped cosine pulses. As can be seen in Fig. 6, the closed loop system has two equilibrium points and the operation is oscillating between the two points. Both of the equilibrium points are stable. However, the operation between these two equilibrium points is oscillatory and yet stable.

Because of this behavior, there are offsets from the reference signals. The output voltage ripple is a function of the circuit parameters. Stability analysis does not

determine the output voltage ripple. Hence, the circuit differential equations need to be solved to predict the output voltage ripple. Simulation results of the output voltage variation after a step load change of 30% to 65% of full-load: Magnetic stimulation pulse train and PWM. Continuing the same procedure for a sense cycle, we can easily get that the total changes of the output voltage after applying a sense pulse is equal to the load resistance are sketched in fig. 9. As we can observe, the control scheme tries to regulate the output voltage by generating the right number of sense and power pulses in each regulation cycle. In addition, this switching point is always reached just after the transformer has reset allowing the circuit to operate very close to the critical conduction mode, where the switch is turned on immediately after reset optimizing circuit efficiency and reducing the size of the transformer.

On each power pulse, a transcranial magnetic stimulation pulse train waits for the auxiliary voltage to drop below zero. This indicates that the converter is in the post-conduction resonance. After this event, the controller waits an additional that will take the voltage across the switch to its minimum level, then turns on the switch for the next cycle. Given the geometry of the resonant signal, this estimate has high accuracy because this information is already measured during the last sense pulse.

Which is a transcranial magnetic stimulation pulse train controller. The off time voltage across the switch in flyback converter is equal to. This number will also make the current of magnetizing inductance be nearly symmetric, hence, causing less current stress for the circuit components. The minimum value of the load resistance at full load is equal to using for can be calculated as, this value also meets the switch current ratings. results of the output voltage ripple for a 30% to 65% step load change. The horizontal arrow shows the output voltage dc level, which is 600 V, whereas the vertical arrow specifies the instant at which the step change is applied.

IV. EXPERIMENTAL RESULTS

As we already mentioned, the peak inductor current in a power pulse is times the peak inductor current in a sense fig 6. Output voltage ripple for a step load change of 30% to 65% of full load. Pulse; therefore, a sense pulse delivers as much power as a power pulse.

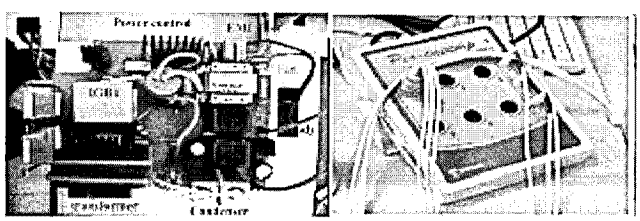

Fig. 7 Experimental tool (power unit and interface: EMG)

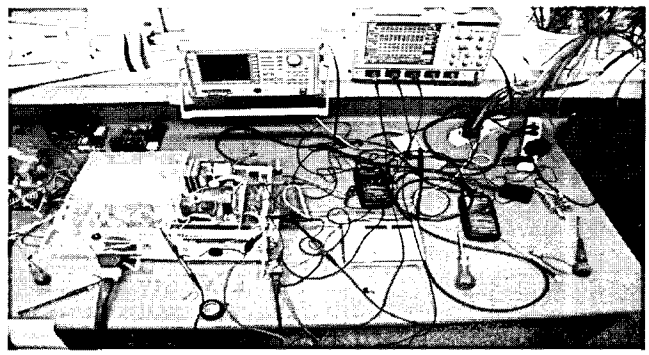

Fig. 8 Experimental based Rogowski-coil frame

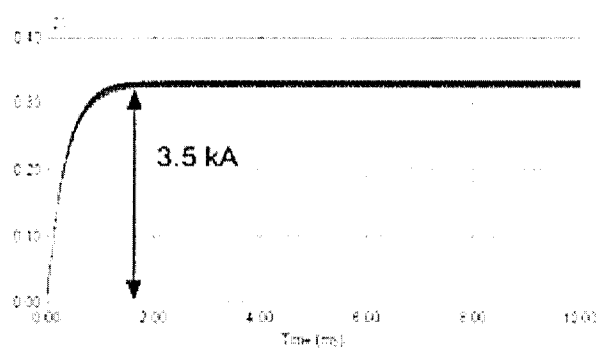

Fig. 9 Experimental simulation waveforms for discharge voltage (3.5kA)

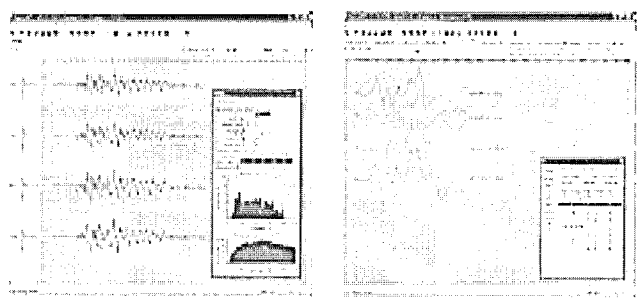

Fig. 10 Experimental based EMG-GUI (low & high stimulator frame)

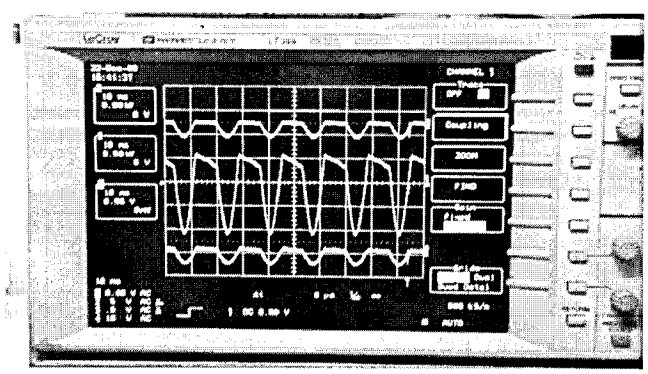

Fig. 11 Experimental flyback waveform (primary and second)

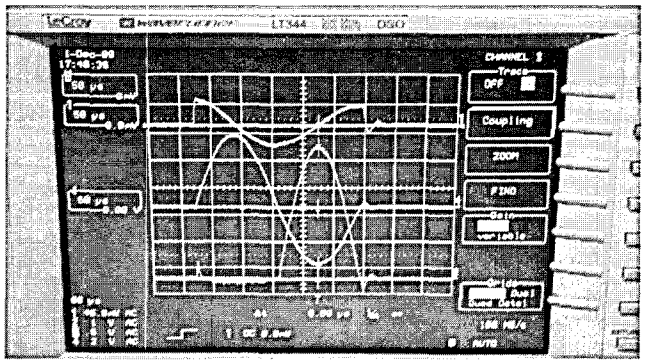

Fig. 12 Experimental waveform of stimulation up current

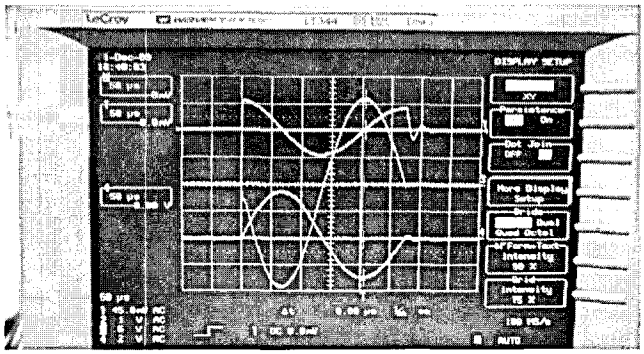

Fig. 13 Experimental waveform of stimulation down current

Fig 7 presented Experimental power unit and interface: EMG. Fig 8 indicated experimental based rogowski-coil frame, Fig 9 presented experimental simulation waveforms for discharge voltage, Fig 10 indicated experimental based EMG-GUI. Fig 11 showed experimental flyback waveform , Fig 12 indicated experimental waveform of stimulation up current, Fig. 13 presented experimental waveform of stimulation down current. A continuous stream of sense pulses thus delivers of the full load. If the load is lighter than this level, the controller enters Smart, when the circuit alternates between the sense pulses and no pulses at all. This mode is similar to pulse skipping techniques. The controller decides to enter the smart-skip mode when the sense pulses reveal that the output voltage is remaining above the desired level, though no power pulses have been sent recently.

The first power pulse shows a clean current ramp; but, the drain voltage reflects the fact that the transformer does not reset by the time the second pulse arrives and, thus, operating in continuous conduction mode. This is also shown in the current on the second pulse, which starts at a non zero value. However, the controller's peak current limiting causes the second power pulse to be much shorter than the first one.

V. CONCLUSION

Flyback power converter has found its way into many applications. To address the challenge of designing a simple controller for this type of converters, this paper introduces the new a Transcranial Magnetic Stimulation Pulse Train control technique. This control method has several advantages over conventional techniques, such as simplicity, accuracy, and fast transient response. Simulation as well as experimental results completely match with the theoretical concept..

REFERENCES

[1] Adachi Y, Miyamoto M, Kawai J, Uehara G. Measurement of spinal cord evoked magnetic .elds by vector SQUID biomagnetometer. Electr Eng Jpn 2006;157(2):15.23.

[2] Akaike T. Comparison of neuronal composition of the vestibulospinal system between cat and rabbit. Exp Brain Res 1973;18(4):429.32.

[3] Barone R, Pavaux C, Blin PC, Cuq P. Atlas d'anatomie dulapin. Paris: Masson et Cie; 1973.

[4] Bernhard CG. The spinal cord potentials in leads from the cord dorsum in relation to peripheral source of a.erent stimulation. Acta Physiol Scand (Suppl.) 1953;106:1.29.

[5] Cohen D. Magnetoencephalography: detection of magnetic. elds produced by alpha rhythm currents. Science 1968;161:778.86.

[6] Cracco RQ. Spinal evoked response: peripheral nerve stimulation in man.

[7] Electroencephalogr Clin Neurophysiol 1973;35:379.86.

[8] Eccles JC, Kostyuk PG, Schmidt RF. Central pathways responsible for MEG vector beamformer technique. IEEE Trans Biomed Eng 2001;48(7):760.71.

[9] Sekihara K, Sahani M, Nagarajan SS. Localization bias and spatial resolution of adaptive and non-adaptive spatial .lters for MEG source reconstruction. Neuroimage 2005;25:1056.67.

[10] Sekihara K, Hild KE, Nagarajan SS. A novel adaptive beamformer for MEG source reconstruction e.ective when large background brain activities exist. IEEE Trans Biomed Eng 2006;35(9):1755.64.

[11] Shimoji K, Kano T, Higashi H, Morioka T, Henschel EO. Evoked spinal electrogram recorded from epidural space in man. J Appl Physiol 1972;33:468.71.

[12] Shimoji K, Matsuki M, Shimizu H. Wave-form characteristics and spatial distribution of evoked spinal electrogram in man. J Neurosurg 1977;46:304.13.

[13] Trahms L, Erne' SN, Trontelji Z, Curio G, Aust P. Biomagnetic functional

[14] A. T. Barker, R. Jalinous, and I. L. Freeston, "Non-invasive magnetic stimulation of human motor cortex [letter]," *Lancet*, vol. 1, pp. 1106–1107, 1985.

[15] E. M. Wassermann, "Risk and safety of repetitive transcranial magnetic stimulation: Report and suggested guidelines from the International Workshop on the Safety of Repetitive Transcranial Magnetic Stimulation, June 5–7, 1996," *Electroencephalogr. Clin. Neurophysiol.*, vol. 108, pp. 1–16, 1998.

[16] M. I. Polkey, Y. Luo, R. Guleria, C. H. Hamnegard, M. Green, and J. Moxham, "Functional magnetic stimulation of the abdominal muscles in humans," *Amer. J. Respir. Crit. Care Med.*, vol. 160, pp. 513–522, 1999.

[17] V. W. Lin, V. Wolfe, F. S. Frost, and I. Perkash, "Micturition by functional magnetic stimulation," *J. Spinal Cord Med.*, vol. 20, pp. 218–226, 1997.

[18] D. Kyroussis, M. I. Polkey, G. H. Mills, P. D. Hughes, J. Moxham, and M. Green, "Simulation of cough in man by magnetic stimulation of the thoracic nerve roots," *Amer. J. Respir. Crit. Care Med.*, vol. 156, pp. 1696–1699, 1997.

[19] V.Walsh and M. Rushworth, "A primer of magnetic stimulation as a tool for neuropsychology," *Neuropsychologia*, vol. 37, pp. 125–135, 1999.
[20] N. T. Galloway, R. E. El Galley, P. K. Sand, R. A. Appell, H.W. Russell, and S. J. Carlan, "Extracorporeal magnetic innervation therapy for stress urinary incontinence," *Urology*, vol. 53, pp. 1108–1111, 1999.

AUTHOR

Whi-Young Kim

INTERNATIONAL JOURNAL OF KIMICS 2008.12, Vol. 7 -2